HHS Public Access

Author manuscript

J Cell Physiol. Author manuscript; available in PMC 2018 January 01.

Published in final edited form as:

J Cell Physiol. 2017 January ; 232(1): 14–18. doi:10.1002/jcp.25384.

Dissection of individual prostate lobes in mouse models of prostate cancer to obtain high quality RNA

Areg Zingiryan, MD[1,2,†], **Nicholas H Farina, PhD**[1,*,†], **Kristiaan H Finstad**[1], **Janet L Stein, PhD**[1], **Jane B Lian, PhD**[1], and **Gary S Stein, PhD**[1]

[1]Department of Biochemistry and University of Vermont Cancer Center, University of Vermont College of Medicine, Burlington, VT USA

Abstract

Genetically engineered mouse models of prostate cancer allow for study of disease progression from localized tumor formation through distal metastasis. The anatomy of the mouse prostate differs dramatically from the human prostate, being composed of four lobe pairs (anterior, dorsal, lateral, and ventral), making the identification and dissection technically challenging. Although the entire murine prostate and surrounding tissue, including urethra, bladder, seminal vesicles, and associated adipose tissue, can be quickly dissected for *en bloc* analysis, it is necessary to isolate individual prostate lobes for gene expression studies elucidating the molecular mechanisms of prostate cancer. The procedure as described here includes full color images, allowing the researcher to appreciate the unique prostate morphology and tissue manipulation required to harvest individual prostate lobes. Along with removing all extraneous tissue, the procedure allows for direct comparison of the different prostate lobes by established downstream techniques. Importantly, high quality RNA required for next-generation gene expression analysis can only consistently be obtained from ventral and lateral lobes. Finally, preclinical studies using prostate targeted therapies can be monitored specifically in individual prostate lobes on the histological and gene expression studies.

Keywords

Prostate Cancer; Prostate Lobe Dissection; Mouse Models; RNA Integrity

INTRODUCTION

Prostate cancer (PCa) is the most diagnosed cancer among men in the United States and is the second leading cause of cancer-related death (Kohler et al., 2015). Currently, there is a gap in knowledge related to the mechanisms of indolent versus clinically relevant disease.

[*]**Corresponding author:** Nicholas H Farina, University of Vermont, 89 Beaumont Avenue, E209 Given Building, Burlington, VT 05405, Phone: (802) 656-4878, Fax: (802) 656-8216, nicholas.farina@med.uvm.edu.

[2]Dr. Zingiryan's present address is: Department of Medicine, Internal Medicine, Lewis Katz School of Medicine, Temple University, Philadelphia, PA USA

[†]These authors contributed equally to this work.

CONFLICT OF INTEREST:

The authors have no conflicts of interest to declare.

Although *in vitro* studies have elucidated numerous biological pathways that regulate prostate cancer cell phenotypes (Fang and Gao, 2014), *in vivo* small animal models are needed to fully understand the complexities of PCa disease progression. Mouse models also allow for developing therapeutic approaches for early intervention and testing treatment strategies.

As mice do not normally develop prostate lesions in their lifespan (Suwa et al., 2002), genetically engineered mouse (GEM) models with prostate-specific altered gene expression have been developed. These include overexpression of oncogenes (eg c-Myc (Ellwood-Yen et al., 2003)), loss of tumor suppressors (eg PTEN (Wang et al., 2003)), deregulation of growth factor and hormone signaling (eg AR (Stanbrough et al., 2001)), and expression of the SV40 T antigen (eg TRansgenic Adenocarcinoma of the Mouse Prostate (TRAMP) (Greenberg et al., 1995; Gingrich et al., 1996)). No GEM model develops all the hallmarks of human prostate cancer, yet the prostate glands of these animals develop primary prostate tumors with phenotypic changes similar to human PCa disease with the formation of PIN lesions, transition to hyperplasia and neoplasia, progression to adenocarcinoma or neuroendocrine disease, invasion of the surrounding tissue, and metastasis (reviewed in (Shappell et al., 2004; Jeet et al., 2010; Irshad and Abate-Shen 2013; Ittmann et al., 2013)). Gene expression studies of GEM prostates isolated at various stages of disease will identify the cellular and molecular changes that occur throughout PCa.

Dissection of the mouse prostate is challenging due to its distinct anatomy (Hurwitz et al., 2001). The human prostate gland is alobular, consisting of three zones, a peripheral, transitional, and central, with the majority of PCa occurring in the peripheral zone (Shappell et al., 2004). The mouse prostate, on the other hand, is divided into four pairs of lobes, anterior, dorsal, lateral, and ventral, individually encapsulated in a thin mesothelial membrane, making identification of the lobes difficult (Hurwitz et al., 2001; Shappell et al., 2004). In addition, the tissue is fragile with little connective tissue, stroma, or vasculature, appearing as a “bag of worms”. There is no difference in cell types between mouse lobes and human prostate zones and no direct evidence suggests that a relationship exists between individual mouse lobes and human prostate zones (Shappell et al., 2004; Ittmann et al., 2013).

Efficient and timely dissection of the mouse prostate is imperative for gene expression studies, paying careful attention to remove surrounding non-prostate tissue and not to puncture nearby fluid-containing organs, which would lead to contamination by bodily fluids. In contrast to a recent review of the mouse prostate anatomy and dissection (Oliveira et al. 2016), our approach avoids interfering with the pelvic organs, especially the urogenital system (UGS), until all the components of the UGS can be properly observed, thereby reducing potential damage to the prostate lobes. Here, we describe a simplified and detailed protocol with full color images that provide straight-forward dissection of individual mouse prostate lobes and isolation of non-degraded RNA for global gene expression studies.

MATERIALS AND METHODS

Ethics Statement

All animals were housed in a pathogen-free environment and handled according to protocol number 12–054 approved by the Institutional Animal Care and Use Committee at the University of Vermont. In conducting research using animals, the investigators adhere to the laws of the United States and regulations of the Department of Agriculture.

Preparation for prostate dissection

A step-wise procedure and associated figure as included as Supplement 1: Prostate Dissection Procedure. The following set-up of reagents, supplies, and instruments is recommended prior to dissection. Sterilize all instruments, petri dishes, and work areas with 70% ethanol. Add 40–50 mL 1× PBS into two 100 mm × 20 mm glass petri dishes and 5–8 mL 1× PBS into four 60 mm × 15 mm glass petri dishes. A ruler may be affixed to the underside of these dishes to allow for tissue measurement. Label each small petri dish as ventral, lateral, anterior, or dorsal. Assure that work areas are adequately lit. The use at least two 60-Watt equivalent light sources above the dissection area and a dual fiber optic light source for the dissecting microscope is necessary. A Leica (Wetzlar, Germany) dissection microscope (Model M165FC) was used for removal of adipose tissue and for dissection of individual lobes.

RNA isolation

Prostate lobes were washed in 1× PBS and transferred to 1 mL QIAzol (QIAGEN, Germantown, MD) for tissue homogenization. Tissue was homogenized on ice in 3 to 6 5-second bursts with a Polyrone 2100 homogenizer with a 7mm tip on setting 25. Homogenized tissue in QIAzol was stored at −80°C until RNA isolation. RNA was isolated with the miRNeasy mini kit (QIAGEN) following manufacture's protocol. RNA quality was assessed on an Agilent (Santa Clara, CA) 2100 Bioanalyzer using RNA Nano chips based on the RIN number, ratio of 28S/18S, and presence of distinct of 18S and 28S peaks with lack of RNA fragments less than 1000 nucleotides.

Quantitative RT-PCR

cDNA for miRNA and mRNA was prepared separately using 1000ng of RNA. MiRNA cDNA was made with the miScript II RT Kit (QIAGEN) using the HiSpec buffer and mRNA cDNA with the SuperScript III First-Strand Kit (Thermo Fisher Scientific, Waltham, MA) following the recommended manufacturer's protocol. All qPCR was performed in 384-well plates on an ABI ViiA7 machine (Thermo Fisher Scientific) using iTaq Universal SYBR Green (BioRad) Hercules, CA or QuantiTect SYBR Green (QIAGEN) for mRNA and miRNA respectively. Data were normalized to expression of HPRT1 (Forward 5' - TCAGTCAACGGGGGACATAAA - 3', Reverse 5' - GGGGCTGTACTGCTTAACCAG - 3') and U6 (5' - ACGCAAATTCGTGAAGCGTTCCATATT - 3').

RESULTS AND DISCUSSION

Requirements for murine prostate dissection

Murine prostate anatomy differs dramatically from the human prostate, being composed of four pairs of individual lobes, anterior, dorsal, lateral, and ventral. Dissection of all eight mouse prostate lobes is technically challenging due to the size and fragility of the tissue (Shappell et al., 2004; Hurwitz et al., 2001). The reader is referred to Supplement 1 for a detailed dissection. Here, we present a brief commentary on key aspects of the procedure.

The murine prostate is very difficult to visualize with the naked eye as each lobe is only several millimeters in size, is covered with adipose tissue, and circumferentially surrounds the junction where the urinary bladder and urethra meet (Figure 1A, B). Prostate lobes are different in consistency and appearance than the surrounding tissue, being translucent and white, resembling a “bag of worms” of opaque tubular glands encapsulated by transparent connective tissue (Figure 1A-C). There are subtle dividing points between each lobe that can be uncovered by applying minimal pressure on the lobes themselves with closed superfine forceps. Furthermore, there are degrees of anatomical variation as no two prostate organs in similar mice will appear identical. Thus, before attempting the entire procedure, it is recommended to closely examine the isolated urogenital tract under a dissecting microscope from a healthy animal to learn the procedure and become adept at dissection, as timing is essential for carrying out molecular studies.

It is possible to dissect the prostate lobes in any order. However, to ensure minimal tissue damage, we recommend beginning with the ventral, proceeding to the lateral and anterior, and ending with the dorsal lobe. It is critical that the lobes are removed intact and free of surrounding connective and adipose tissue. Each set of prostate lobes is unique in size, with the anterior lobes being the largest and lateral lobes the smallest (Figure 1D). Both healthy and tumorigenic prostates can be harvested following the supplemental protocol from a wide age-range of animals (6 weeks through 33+ weeks). It is important to note that while healthy prostates are delicate translucent tissues, prostate lobes from GEM models, especially in aged animals, are opaque with more vasculature and connective tissue making them less fragile (Figure 1E). In many cases, intra-prostatic tumors are obvious. Dissection of all eight prostate lobes is typically performed within an hour of animal sacrifice. However, the entire urogenital system can be isolated and snap-frozen or placed in fixative for *en bloc* histologic analysis within 5–10 minutes (Hurwitz et al., 2001). In addition, the ventral and lateral lobes can be harvested within 20 minutes and prepared for gene expression analysis to elucidate the molecular mechanisms of prostate cancer progression.

Ventral and lateral but not dorsal or anterior prostate lobes yield high quality RNA

Once removed, all lobes may be processed for protein expression analysis or fixed for histologic and imaging procedures. However, RNA isolated from the entire prostate (all lobes combined without individual lobe dissection) yields poor quality RNA (Figure 2A). We identified several factors leading to RNA decay, including time of dissection, rupture of the urinary bladder or seminal vesicles and contamination by the associated fluids, or contamination from non-prostate tissue. We assessed RNA quality in each set of lobes

dissected within 20, 30, 40, and 60 minutes from animal sacrifice to determine if RNA stability depended on lobe of origin or processing time (Figure 2B–H): Dissected tissue was submerged in 1 × PBS prior to homogenization at the appropriate time point. RNA isolated from the anterior lobes is always degraded, even when the tissue is harvested and processed for RNA isolation within 20 minutes (Figure 2B). When the dorsal lobe is isolated within 20 minutes, little RNA degradation is seen yet if the time to tissue processing for RNA reaches 30 minutes, RNA degradation may occur (Figure 2C, D). However, RNA isolated from either ventral or lateral lobes, homogenized separately or together as ventral and lateral, results in good quality RNA, even when processed for RNA one hour from time of sacrifice (Figure 2E–H). Each of the murine prostate lobes in GEMs develops human-like prostatic tumors with similar cell types found in both mouse and human tissue, and there is no direct evidence suggesting a difference exists between individual mouse lobes and human prostate zones (Shappell et al., 2004; Ittmann et al., 2013). As such, it is recommended that only the ventral and lateral lobes be used for RNA isolation and that ventral and lateral lobes be combined prior to tissue homogenization to account for any potential differences between lobes. Both miRNA and mRNA can be reproducibly detected in RNA isolated from the ventral and lateral prostate lobes. Here, we present representative qPCR data of an mRNA that is elevated in the ventral and lateral prostate lobes of transgenic TRAMP animals as compared to non-transgenic controls (Figure 3A). We interrogated the levels of a miRNA that targets the assayed mRNA and observe reciprocal downregulation in TRAMP prostates (Figure 3B).

Critical steps within the protocol—Prior to animal sacrifice, take care to set up an organized workspace for improved efficiency, sample quality, and overall time of procedure. It is critical to be able to quickly identify the prostate lobes and become familiar with the overall consistency of the tissue, as they are very fragile, delicate structures that are easily damaged. The prostate lobes circumferentially surround the junction where the urinary bladder and urethra meet under layers of fat and connective tissue.

During the gross dissection, it is particularly beneficial to keep the drained urinary bladder elevated as much as possible. The urinary bladder is composed of very strong musculature and is resistant to tension. Thus, you can grab and pull on it with a considerable amount of force without fear of tearing as long as serrated forceps are used.

The goal of the microscopic dissection is to remove 80–90% of each prostate lobe since each lobe is implanted within the urethra. Therefore, a more superficial approach to dissecting out the lobes allows for a greater chance to isolate high quality and pure tissue. The most important concept is that the fine dissection is based on finesse, not force, with short incremental movements. Instead of grasping the lobes themselves, carefully shear the transparent connective tissue surrounding the lobes apart until they are free from all attachments and can be easily cut at the base of origin at the urethra. The type of scissors used to remove the prostate lobes is based on personal preference and variation in anatomy. Use of scissors with both a small (~2.5mm) and large (~7mm) cutting edge is advantageous when working in tightly packed or well dispersed tissue, respectively. In addition, having an absorbent material nearby allows for casual cleaning of the forceps and scissors during the fine dissection. Lastly, there are rare cases in which the ventral lobe is tightly fused to the

lateral lobe and not separable. This usually is a unilateral event and is unlikely to occur bilaterally.

Modifications and limitations—Once the procedure is mastered with efficient removal of the prostate lobes, the harvest of other tissues can be easily accomplished including lymph nodes, liver, and lung in metastatic prostate cancer mouse models as well as cardiac puncture for whole blood, serum, or plasma. In addition, the procedure can be modified to remove only select prostate lobes. The limitations of the procedure are mostly related to experience, with more repetition leading to improved efficiency and quality. Due to the size and frailty of the prostate, it may not be possible to isolate individual lobes from mice younger than 6 weeks.

Significance and future applications—This technique describes the isolation of individual prostate lobes allowing for intra- and inter- lobe comparison as well as full color images of each murine prostate. Once the technique has been mastered, the prostate lobes can be isolated from a multitude of GEM prostate cancer models. In addition, these data identify a need to use only the lateral and ventral lobes for transcriptome analysis. Full gene expression analysis can be performed and the molecular mechanisms of prostate cancer progression elucidated. Finally, preclinical studies using prostate targeted therapies can be monitored specifically in individual prostate lobes on the histological and gene expression levels.

Supplementary Material

Refer to Web version on PubMed Central for supplementary material.

Acknowledgments

The authors thank the Lake Champlain Cancer Research Organization, National Cancer Institute (P01 CA140043-06), and National Institute of Dental and Craniofacial Research(R37 DE012528-32) for funding. The U.S. Army Medical Research Acquisition Activity, 820 Chandler Street, Fort Derrick MD 21702-5014 is the awarding and administering acquisition office. This work was supported by the Office of the Assistant Secretary of Defense for Health Affairs, Through the Prostate Cancer Research Program under Award No. W81XWH-14-1-0468. Opinions, interpretations, conclusions and recommendations are those of the author and not necessarily endorsed by the Department of Defense.

LITERATURE CITED

Ellwood-Yen K, Graeber TG, Wongvipat J, Iruela-Arispe ML, Zhang J, Matusik R, Thomas GV, Sawyers CL. Myc-driven murine prostate cancer shares molecular features with human prostate tumors. Cancer Cell. 2003; 4:223–238. [PubMed: 14522256]

Fang YX, Gao WQ. Roles of microRNAs during prostatic tumorigenesis and tumor progression. Oncogene. 2014; 33:135–147. [PubMed: 23455326]

Gingrich JR, Barrios RJ, Morton RA, Boyce BF, DeMayo FJ, Finegold MJ, Angelopoulou R, Rosen JM, Greenberg NM. Metastatic prostate cancer in a transgenic mouse. Cancer Res. 1996; 56:4096–4102. [PubMed: 8797572]

Greenberg NM, DeMayo F, Finegold MJ, Medina D, Tilley WD, Aspinall JO, Cunha GR, Donjacour AA, Matusik RJ, Rosen JM. Prostate cancer in a transgenic mouse. Proc Natl Acad Sci U S A. 1995; 92:3439–3443. [PubMed: 7724580]

Hurwitz AA, Foster BA, Allison JP, Greenberg NM, Kwon ED. The TRAMP mouse as a model for prostate cancer. Curr Protoc Immunol. 2001; Chapter 20(Unit 20.5)

Irshad S, Abate-Shen C. Modeling prostate cancer in mice: something old, something new, something premalignant, something metastatic. Cancer Metastasis Rev. 2013; 32:109–122. PMC3584242. [PubMed: 23114843]

Ittmann M, Huang J, Radaelli E, Martin P, Signoretti S, Sullivan R, Simons BW, Ward JM, Robinson BD, Chu GC, Loda M, Thomas G, Borowsky A, Cardiff RD. Animal Models of Human Prostate Cancer: The Consensus Report of the New York Meeting of the Mouse Models of Human Cancers Consortium Prostate Pathology Committee. Cancer Res. 2013; 73:2718–2736. [PubMed: 23610450]

Jeet V, Russell PJ, Khatri A. Modeling prostate cancer: a perspective on transgenic mouse models. Cancer Metastasis Rev. 2010; 29:123–142. [PubMed: 20143131]

Kohler BA, Sherman RL, Howlader N, Jemal A, Ryerson AB, Henry KA, Boscoe FP, Cronin KA, Lake A, Noone A-M, Henley SJ, Eheman CR, Anderson RN, Penberthy L. Annual Report to the Nation on the Status of Cancer, 1975–2011, Featuring Incidence of Breast Cancer Subtypes by Race/Ethnicity, Poverty, and State. Journal of the National Cancer Institute. 2015; 107

Oliveira DS, Dzinic S, Bonfil AI, Saliganan AD, Sheng S, Bonfil RD. The mouse prostate: a basic anatomical and histological guideline. Bosn J Basic Med Sci. 2016; 16:8–13. [PubMed: 26773172]

Shappell SB, Thomas GV, Roberts RL, Herbert R, Ittmann MM, Rubin MA, Humphrey PA, Sundberg JP, Rozengurt N, Barrios R, Ward JM, Cardiff RD. Prostate Pathology of Genetically Engineered Mice: Definitions and Classification. The Consensus Report from the Bar Harbor Meeting of the Mouse Models of Human Cancer Consortium Prostate Pathology Committee. Cancer Res. 2004; 64:2270–2305. [PubMed: 15026373]

Stanbrough M, Leav I, Kwan PW, Bubley GJ, Balk SP. Prostatic intraepithelial neoplasia in mice expressing an androgen receptor transgene in prostate epithelium. Proc Natl Acad Sci U S A. 2001; 98:10823–10828. [PubMed: 11535819]

Suwa T, Nyska A, Haseman JK, Mahler JF, Maronpot RR. Spontaneous lesions in control B6C3F1 mice and recommended sectioning of male accessory sex organs. Toxicol Pathol. 2002; 30:228–234. [PubMed: 11950166]

Wang S, Gao J, Lei Q, Rozengurt N, Pritchard C, Jiao J, Thomas GV, Li G, Roy-Burman P, Nelson PS, Liu X, Wu H. Prostate-specific deletion of the murine Pten tumor suppressor gene leads to metastatic prostate cancer. Cancer Cell. 2003; 4:209–221. [PubMed: 14522255]

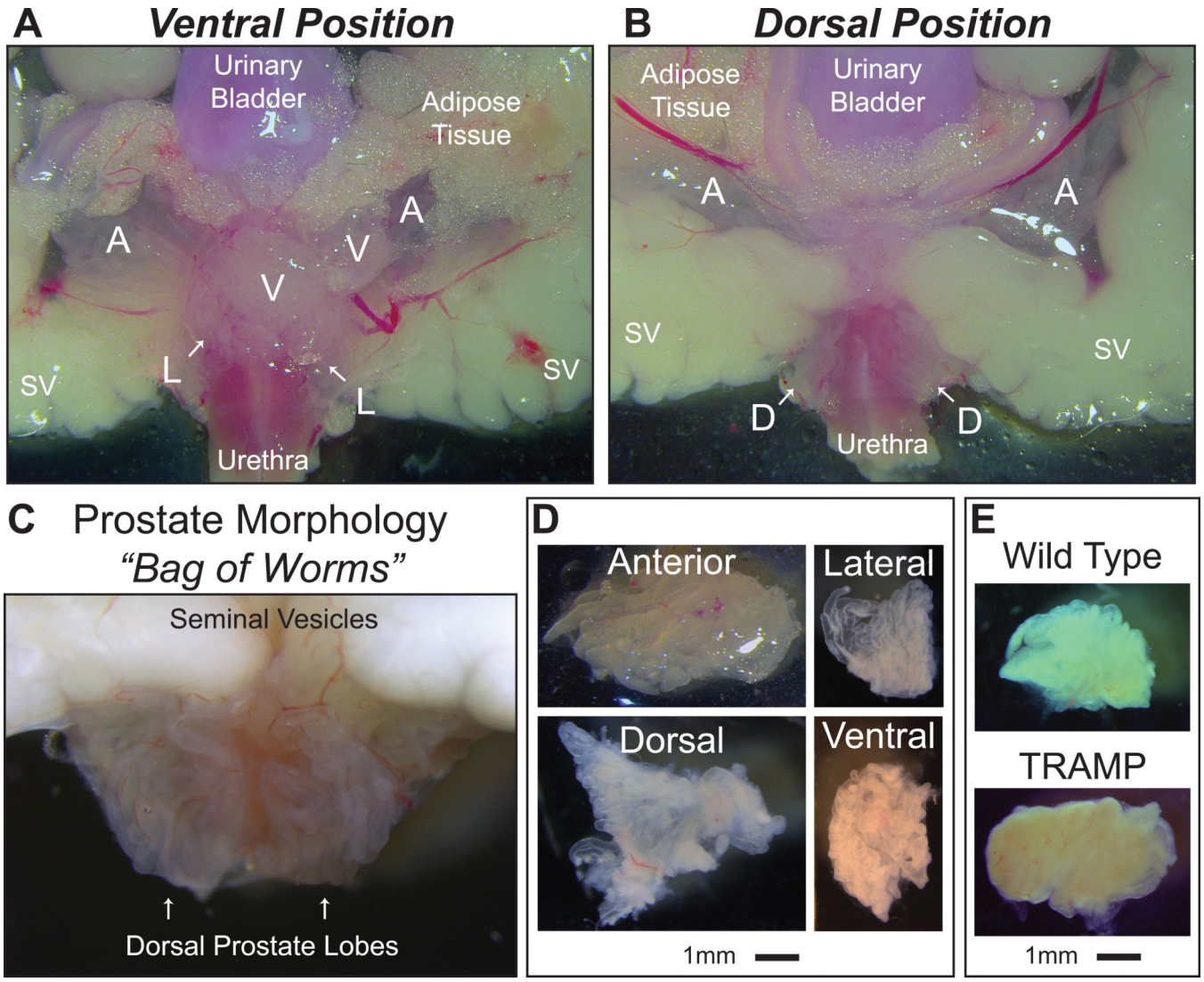

Figure 1. Anatomy of murine prostate lobes

(A) *Ventral Position:* The anterior (A), lateral (L), and ventral (V) prostate lobes surround the urethra and lie directly adjacent to the urinary bladder, seminal vesicles (SV), and accompanying adipose tissue as seen in the ventral position. **(B)** *Dorsal Position:* The anterior (A) and dorsal (D) prostate lobes lie on opposite sides of the seminal vesicles (SV) as seen in the dorsal position. **(C)** The "bag of worms" morphology of white, translucent tubes allows the prostate to be easily distinguished from adjacent tissue. The urethra can be seen in pink directly behind the translucent dorsal prostate. **(D)** Representative images of prostate lobes isolated from wild type animals showing translucence, whiteness in color, and size, ranging from 3 to 8 mm. **(E)** The lateral lobe of a 33 week old wild type or TRAMP animal illustrates the difference in tissue color and density typical of a diseased prostate. Note the opaqueness. Scale bar is 1mm.

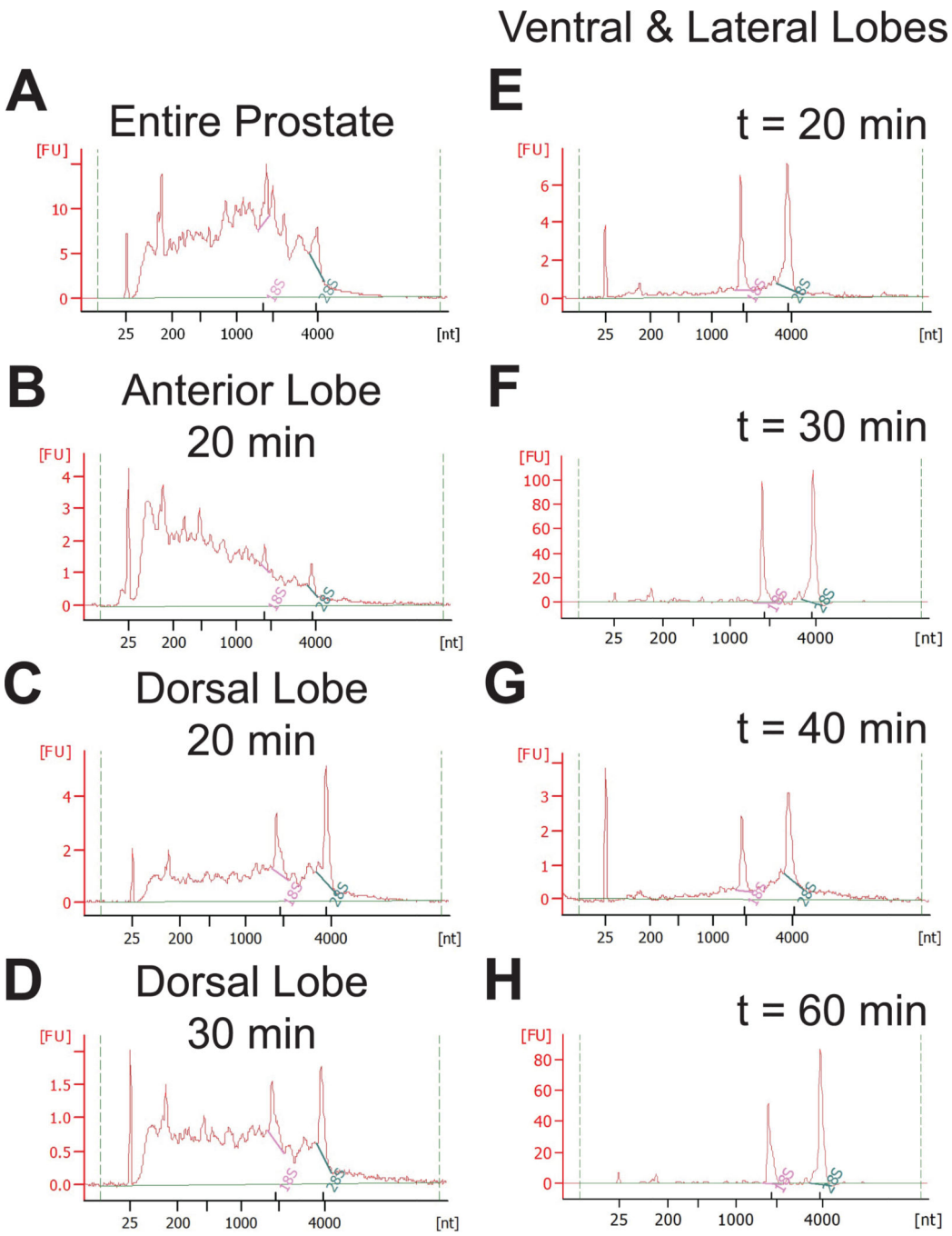

Figure 2. RNA quality depends on the prostate lobe of origin

The quality of RNA, isolated by conventional methods as assessed on a bioanalyzer, is dramatically different based on lobe and time from animal sacrifice to tissue homogenization **(A–H)**. The lack of distinct 18S and 28S peaks in the entire prostate **(A)** or anterior lobe **(B)** with a broad peak between 25nt and 4000nt indicates RNA decay. Homogenization of the dorsal lobe within 20 minutes of mouse sacrifice results in usable RNA **(C)** but the RNA is unstable and becomes degraded when this time is extended to 30 minutes **(D)**. Note the difference in the ratio between 18S and 28S peaks. Good quality RNA is obtained from both

ventral and lateral lobes when tissue homogenization occurs at 20 minutes **(E)**, 30 minutes **(F)**, 40 minutes **(G)**, and 60 minutes **(H)** from time of death. While (**E–H**) depict RNA quality from ventral and lateral lobes processed together, the same results are found when ventral and lateral lobes are processed separately. The relative fluorescence units (FU) scale depends on input RNA concentration and should not be compared here. RNA may be diluted (1:2–1:10) prior to quality assessment. The larger FU range in (**F**) and (**H**) is from undiluted RNA. Each graph represents RNA isolated from different prostate lobes and processed uniquely.

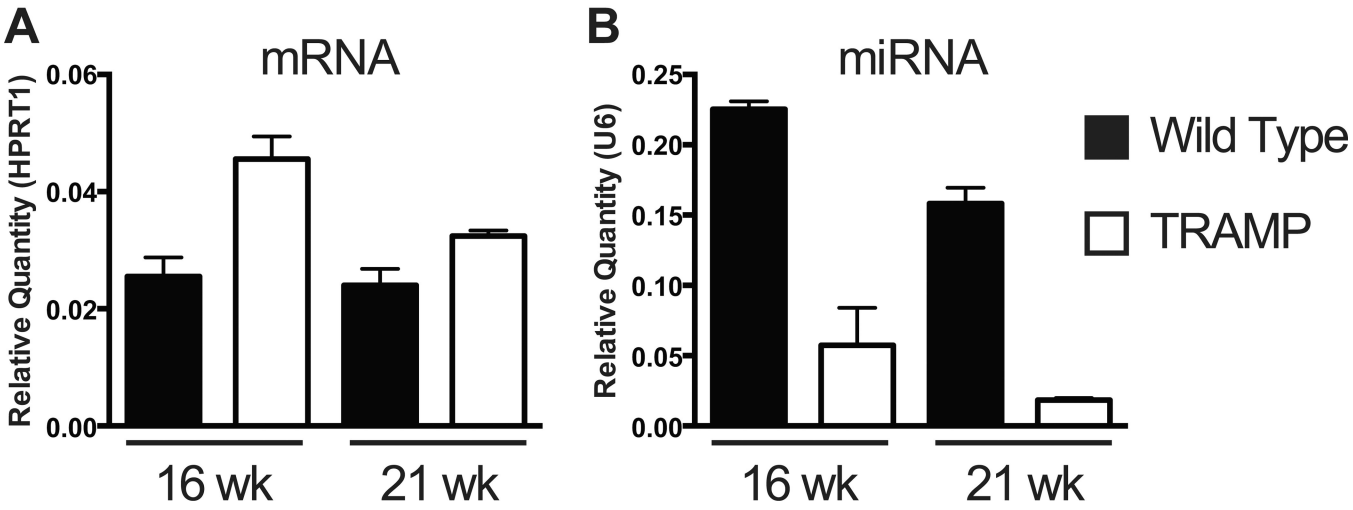

Figure 3. Example expression of mRNA and miRNA in ventral and lateral prostate lobes

Representative qRT-PCR of **(A)** mRNA and **(B)** miRNA from total RNA isolated from the ventral and lateral prostate lobes of wild type or age-matched TRAMP animals at 16 and 21 weeks of age. mRNA expression is normalized to HPRT1 and miRNA expression normalized to U6. N = 3 animals at each time point. Error bars are SEM.